ELSEVIER

Contents lists available at ScienceDirect

Journal of the European Ceramic Society

journal homepage: www.elsevier.com/locate/jeurceramsoc





An interface nucleation rate limited sintering kinetic model applied to *in situ* sintering Al₂O₃-SmAlO₃ composites

Shen J. Dillon^{a,*}, Yonghui Ma^b, Eric Lang^{c,d}, Jia-hu Ouyang^e, Khalid Hattar^{c,f}

- ^a Department of Materials Science and Engineering, University of California, Irvine, CA 92697, USA
- ^b Yantai Research Institute of Harbin Engineering University, Yantai, Shandong 264006, China
- ^c Materials, Physical, and Chemical Sciences, Sandia National Laboratories, Albuquerque, NM 87185, USA
- ^d Department of Nuclear Engineering, University of New Mexico, Albuquerque, NM 87131, USA
- e School of Materials Science and Engineering, Harbin Institute of Technology, Harbin 150001, China
- f Department of Nuclear Engineering, University of Tennessee, Knoxville, TN 37996, USA

ARTICLE INFO

Keywords: Sintering Al_2O_3 in situ TEM Kinetics

ABSTRACT

A nucleation rate limited sintering model was recently developed based on observations of bicrystal sintering. This work validates the applicability of this model for sintering of polycrystalline clusters of Al_2O_3 -Sm AlO_3 at high temperature in the range of 1130-1610 °C. The model fits the data well and agrees with trends observed during bicrystal sintering. A temperature dependence to the dominant sintering strain deformation modes is observed from *in situ* heating experiments performed in a transmission electron microscope (TEM). The observations provide insights into how temperature influences the early stages of sintering by affecting the pore size distribution through local de-sintering. This provides insights into the role heating rate and sintering schedule play in microstructural evolution that influences the grain size versus density trajectory.

1. Background

Solid-state preparation of bulk materials from powders often requires sintering. The process has gained renewed interest for applications such as densifying 3-D printed colloids or the preparation of solid-state Li-ion batteries [1–3]. A variety of novel sintering techniques have emerged in the past few decades that can promote fine grained dense microstructures, reduce residual stresses, suppress vaporization, or reduce sintering temperature and associated processing costs [3-10]. A common thread within the literature discussing these processes is disagreement about their influence on mechanisms for sintering. Essentially all discussion of oxide sintering kinetics begin with an assumption of diffusion rate limited transport kinetics typically at the grain boundary or surface, but possibly within the lattice [11-16]. Although diffusion limited kinetic models can fit experimental sintering data well, [11,15] alternative models can fit experimental data equally well [17,18]. Diffusional models assume that interfaces active in the sintering process serve as ideal unsaturable sinks for continuous point defect fluxes. Experimental evidence exists to support the idea that many interfaces are good point defect sinks [19-21], while conflicting evidence has been presented for the case of creep [22]. Irradiation experiments utilized in many studies,

however, produce both interstitials and vacancies that can recombine when trapped at interfaces. Experiments based on quenched-in vacancies, typically produce too few defects to test the hypothesis that the interfaces are unsaturable. Such experiments, therefore, do not necessarily provide support for the notion that those interfaces are unsaturable sinks for continuous flux of mass to or from the interface.

A comparison between grain boundary mediated sintering and creep will be considered here to highlight inconsistencies between diffusive models for the two processes. The strain, ε , rate, associated with each process may be written as [11,23];

$$\frac{d\varepsilon_i}{dt} = \frac{K\sigma_i \Omega \delta D_{gb}}{kTr^3} \tag{1}$$

where t is time, K is a geometric constant, σ_i is the stress driving force, Ω is the molecular volume, δ is the grain boundary width, D_{gb} is the grain boundary diffusivity, kT is the thermal energy, r is the particle radius, and the subscript i denotes that these terms could be associated with creep or sintering. At similar stresses, temperatures, and particle sizes, the two processes should yield strain rates of similar magnitude, although the signs of the stress and strain rates are opposite. Fig. 1 plots the stress dependence of creep rate and densification rate for bicrystal

E-mail address: sdillon1@uci.edu (S.J. Dillon).

^{*} Corresponding author.

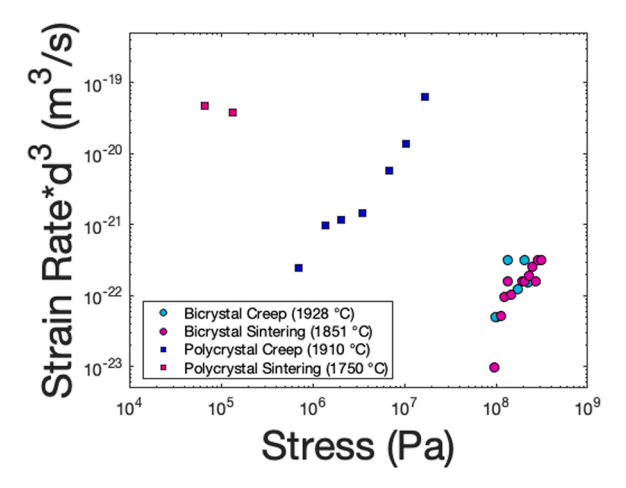


Fig. 1. Comparison between bicrystal and polycrystalline creep and sintering strain rates at their respective driving forces in $\rm ZrO_2$ materials, where the rates are normalized by the grain size cubed. Note that the polycrystalline creep data includes the low stress non-Newtonian regime, an intermediate stress Newtonian regime, and a high stress non-Newtonian regime. The two non-Newtonian regimes are hypothesized to correspond to grain boundary and lattice mediated creep regimes, respectively, while the Newtonian regime should correspond with Coble creep. Data is based on references [37,38,89,90].

and polycrystalline ZrO2 at a range of similar temperatures. The sintering stress is approximated to be on the order of $2\gamma_s/r$. This may slightly underestimate the sintering stress, nevertheless, the kinetics of polycrystalline sintering and creep clearly do not agree well. Bicrystal sintering and creep kinetics do agree well with each other but require significantly larger stresses than both polycrystalline sintering and creep. The creep rate exhibits a non-Newtonian regime at low stresses and a linear regime at intermediate stresses. This non-Newtonian response results from grain boundaries not acting as perfect sinks at low driving forces [22,24,25]. The sintering strain rate significantly exceeds the creep strain, in each case, at stresses of equivalent magnitude. The poor agreement between creep and sintering kinetics is observed for numerous systems [11,26-35]. This comparison would lead one to anticipate that sintering may also exhibit a non-Newtonian response. The sintering data could be compared with the linear creep regime, which is generally thought to correspond with a diffusive grain boundary (GB) mechanism. In this case, the sintering stress is in better agreement with the creep data, but still generally exceeds it. Non-Newtonian sintering has, indeed, been observed in some cases during hot pressing [36]. Comparing strain rates during hot pressing to creep strain rates at similar temperatures, applied stresses, and grain sizes only exacerbates these discrepancies. Furthermore, a threshold stress, necessary to activate interfacial creep, is often reported to be on the order of 106Pa and has been suggested to be associated with activating GB dislocation motion [22,26,27]. This would imply that sintering should not be active at such driving forces, although sintering is commonly reported at average driving forces of that magnitude.

If densification is non-Newtonian in its driving force dependent strain rate, then one might invoke an interface reaction rate limited type kinetic mechanism [18,22]. Two such mechanisms could be active; (1) kinetics rate limited by the emission/absorption of point defects at interfacial line defects that mediate climb or (2) kinetics rate limited by the nucleation of GB dislocations that serve as point defect sources/sinks and climb in response to a flux. Coble [11] considered the former mechanism and noted that it would be indistinguishable from a diffusive mechanism when fitting isothermal data to a constitutive equation. Ashby [22], and later Artz et al. [24], proposed such a mechanism for GB mediated creep, which was also developed by Burton [25]. Burton [25] considered the possibility of a nucleation rate limited mechanism for creep but concluded that the activation energy for GB dislocation

nucleation is too large to enable creep at moderate stresses utilized experimentally. Recent bicrystal creep experiments suggest that interface reaction rate limited kinetics persist up to high stresses, $> 10^8 Pa$ [37,38], see Fig. 1, in systems where diffusive creep is observed in the bulk at $< 10^7 Pa$ [39]. Although a detailed discussion of creep lies outside of the scope of this manuscript, it is noted that stress concentrations within polycrystalline microstructures [40–42] can account for the discrepancy [43].

Recent bicrystal sintering experiments observed nucleation rate limited kinetics up to $\approx 10^8 Pa$ [37,44–46]. Good agreement between creep and sintering were obtained from the bicrystal experiments, both in terms of the diffusivities calculated at high driving forces, consistent with Eq. (1), and the activation volumes describing the stress dependence in the low stress regime [46]. A model for nucleation rate limited sintering mechanism was subsequently proposed, which was informed by results from bicrystal sintering in several systems [46,47]. During bicrystal sintering, the densification occurs discontinuously, while coarsening occurs continuously. When densification is not active, the sintering stress tends to increase, during shrinkage of certain grains, until reaching a critical stress necessary to activate densification, which then occurs at a rate consistent with diffusive kinetics. This critical stress, σ_{sc} , can be defined as;

$$\sigma_{s,c} = \frac{-kT \ln \frac{\dot{\varepsilon}}{\dot{\varepsilon}_0} - H^* + S^* T}{\nu^*}$$
 (2)

where v^* , H^* and S^* are the activation volume, enthalpy and entropy [48]. If $\left\|k\ln\frac{\dot{\varepsilon}}{\dot{\varepsilon}_o}\right\| > S^*$ and H^* is weakly dependent on temperature, then $\sigma_{s,c}$ will decrease with temperature.

Dissipation of surface energy, γ_S , via $dG = \gamma_S d(A/V)$, where (A/V) denotes the surface area per unit volume is hypothesized to provide a driving force to overcome this critical stress. From the activated state, work per volume, $dw = \sigma_S d\varepsilon$ is done to induce densification strain, ε , at the sintering stress, σ_S . These thermodynamic quantities form an equality by the introduction of efficiency terms, ζ and η , in the following form;

$$\frac{d\varepsilon}{d(A/V)} = -\frac{\gamma_S \zeta}{\sigma_{s,c} \eta} \tag{3}$$

where η represents an efficiency of work and was proposed to be of the order $\eta \approx \frac{v_f}{\Omega}$, where v_f is the point defect formation volume [46]. ζ is the efficiency of converting interfacial energy to densification work and it was suggested that $\zeta \approx 1$ based on prior experiments and MD simulations. This is hypothesized to be reasonable when each grain boundary is attached to a pore. Nucleation rate limited kinetics should dominate when $\sigma_{s,c}$ exceeds the average sintering stress that would be anticipated for diffusion limited kinetics to be of the order $\sigma_{s,average} \sim 2\gamma_S/r$. Eq. (3) is purely thermodynamic and will generally be true; however, it is only useful as a predictive equation if $\frac{\zeta}{\eta}$ is within a factor of ≈ 2 –5 of unity or known explicitly. In this model coarsening dominates the densification rate. For the case of coarsening via surface diffusion;

$$r^{4} - r_{o}^{4} = C \frac{D_{s} \gamma_{s} \Omega^{2} \nu}{kT} (t - t_{o}) \tag{4}$$

where C is a geometric constant, D_s is the surface diffusivity, and ν is the concentration of surface defects mediating diffusion [49]. $(A/V) = \frac{B}{r}$, where B is a geometric coefficient. For later stages of sintering, grain growth models could be utilized instead.

This model provides a rationalization for the discrepancies between sintering and creep kinetics, since the densification rate at a particular temperature is determined by the coarsening rate scaled to Eq. (3). Coarsening could occur via a combination of vapor phase transport, surface diffusion, or grain boundary migration. The rates of coarsening via surface diffusion and grain growth should both generally exceed the

rate of grain boundary diffusion at the same average driving force. This could partially explain why the densification rate generally exceeds the creep rate at the same average driving force.

Prior literature often assumed the presence of sinks [11] and suggested that climb mediating grain boundary dislocations pre-exist and can be self-propagating [25], analogous to screw dislocation induced surface steps at free surfaces [50]. Evidence for such defects, however, is generally lacking and, as discussed in prior work [46], the cited examples in the published literature are somewhat inconclusive [51–53]. Indeed, the least intuitive aspect of the model, and indeed sintering in general, relates to the question as to how GB dislocations can nucleate when the critical stress far exceeds the average sintering stress, $\sigma_{\text{S,CV}} \ll \sigma_{\text{S,C}}$. Prior *in situ* bicrystal sintering work [37,44,46] suggests that the local stress can approach $\sigma_{\text{S,C}}$ as the GB area reduces locally. Generally, local increases in the sintering stress might occur as GBs and particles approach topological events that increase the local chemical potential and/or reduce the interfacial area over which the sintering force, i.e. sintering potential [54], is applied.

Prior work [46] has focused on demonstrating the occurrence of nucleation rate limited kinetics during 2-particle sintering experiments and applying the model described in Eqs. (3) and (4) to analyzing such data. A preliminary effort was made to demonstrate that the model could be fit to isothermal sintering of a cluster of particles. The data, however, was insufficient to validate the temperature dependence predicted by the model. The temperature dependence is important because it was hypothesized to explain temperature dependent sintering phenomena of practical interest to processing materials [3-10]. Eq. (2) implies that $\sigma_{s,c}$ will decrease with temperature, which was observed for bicrystal eutectic interfaces between Al₂O₃ and GdAlO₃. The current work extends this analysis to polycrystalline particle clusters of different sizes at different temperatures. A goal of the effort is to understand how mechanistic concepts understood at the bicrystal level extend to the bulk. For example, what conditions in polycrystalline structures drive high local stresses to overcome the large barrier to grain boundary dislocation nucleation. Also, particles exhibit rotation during densification in 2-particle configurations [37,44,46]. Concurrent rotation and densification support the claim that the onset of densification occurs along with the nucleation of a grain boundary dislocation. How such deformation is accommodated in polycrystalline compacts and if a temperature dependence exists is unclear. This work seeks to develop a general understanding of how such a model applies at the polycrystalline level. An immiscible 2-phase system, in this case is investigated here because grain boundary migration will not be the dominant coarsening mechanism. Since Eq. (3) implies that coarsening and densification are inherently coupled, it is convenient to simplify the nature of the coarsening processes in this work. Grain growth may also occur by the nucleation and motion of disconnections [55,56]. The degree to which these processes are competitive, independent, or synergistic, and therefore would influence ζ , remains unclear. Suppressing grain growth enables our analysis to ignore these considerations for now. Al₂O₃-rare earth oxide composites are also of considerable practical interest as high temperature creep resistant structural materials [57-60], often prepared as solidified eutectics or sintered structures near the eutectic composition [61].

2. Experimental procedure

 $Al_2O_3\text{-SmAlO}_3$ nanoparticles were prepared according to the eutectic composition ($Al_2O_3:SmAlO_3=52\text{:}48$ at mol.%) via co-precipitation from a homogeneous solution of water and alcohol containing $Al(NO_3)_3 \bullet 9H_2O$ (99% purity with maximum 0.2% Fe, Tianjin Fuchen Chemical Reagent Co. Ltd., China) and Sm_2O_3 (≥ 99.9 %, Beijing Grirem Advanced Materials Co., Ltd., China) dissolved in dilute nitric acid. Urea or ammonia were utilized to induce precipitation in the presence of small amounts (~1 wt%) of polyethylene glycol, used as a surfactant to

drive flocculation of the precipitates. The material was then centrifuged, dried, and ultimately calcined at $1200\,^{\circ}$ C. Additional details are provided in a previous report [62].

Dimpled and ion milled 3 mm Al_2O_3 disk samples prepared for prior work [63] were used as substrates in this study. These samples were coated on one side with ≈ 3 nm of Iridium to suppress charging in the TEM. The ultrafine Al_2O_3 -SmAlO $_3$ powder was dispersed in water, dropped onto the Al_2O_3 disk, and allowed to dry. Particle clusters deposited at the edge of the hole in the disk were then observed during in situ heating within the transmission electron microscope (TEM). The goal of this preparation method was to deposit clusters of particles that were not constrained in the plane of the observation, which would be the case for particles deposited on a traditional TEM grid. The use of an Al_2O_3 substrate avoids additional chemical interactions and produces grain and phase boundaries at the substrate like those within the nanoscale Al_2O_3 -SmAlO $_3$ cluster.

In situ heating experiments were performed in the I³TEM at Sandia National Laboratories, which is a highly modified JEOL 2100 LaB₆ TEM. A 1064 nm 20 W laser with a $\approx 50 \ \mu m$ spot was used to locally heat the specimen to high temperatures. This method is convenient in this configuration because it can obtain high temperatures and multiple different regions may be sequentially in situ sintered [37,38]. Electron diffraction-based lattice parameter expansion measurements were used as a basis for temperature calibration, see an example in Supplementary Fig. S1. The temperature is anticipated, based on prior experiments [37, 38,64,65], to be approximately linear in applied laser power. This linearity is used to approximate the average temperature. It should be noted that this is only likely accurate to approximately 50 °C, which is why all temperatures are indicated as approximate. The goal of this work is not to quantify kinetic rates exactly at particular temperatures, but is to, instead, understand how relative temperature influences sintering mechanisms. Experiments were performed as a function of beam current density to observe any influence of the electron beam. The sintering kinetics observed herein are generally fast relative to any irradiation induced diffusion that could be caused by displacement damage at the grain boundaries. In addition, the threshold for displacement damage in the lattice is larger than the maximum recoil energy [66]. Charging could influence the sample by driving ionic currents, such as redistribution of mass between the region under the beam and its perimeter as is commonly observed in ionic solutions [67]. No such effects were observed in any imaging conditions used. It was observed that at high electron fluxes, a small amount of Al₂O₃ evaporation was promoted. However, no such evaporation was observed at imaging conditions utilized for the work reported. The role of vacuum pressure on microstructural evolution in Al₂O₃ based materials is somewhat ambiguous, with some conflicting results. Processing such materials under vacuum or H₂ gas, i.e. reducing is common in application, so the experiments can represent realistic environmental conditions.

Data was primarily analyzed using ImageJ. Grain sizes were measured manually based on equivalent area diameter. (A/V) was approximated as the projected particle perimeter divided by its area. The change in density was approximated based on the change in enclosed area, A_{ϵ} , within the boundaries of a cluster of particles. A linear strain was then calculated to be the square root of the area strain, $\varepsilon=\frac{1}{2}$

3. Results

3.1. Behavior of small clusters

Fig. 2 and Video S1 provide an instructive example of sintering of a small cluster of particles at $T\approx 1440\,^{\circ}C.$ Isolated SmAlO $_3$ grains appear darker on average than Al_2O_3 in the bright-field images due to their higher density. For thicker clusters of particles or Al_2O_3 particles oriented near zone axes, this interpretation may not be clear. In this work,

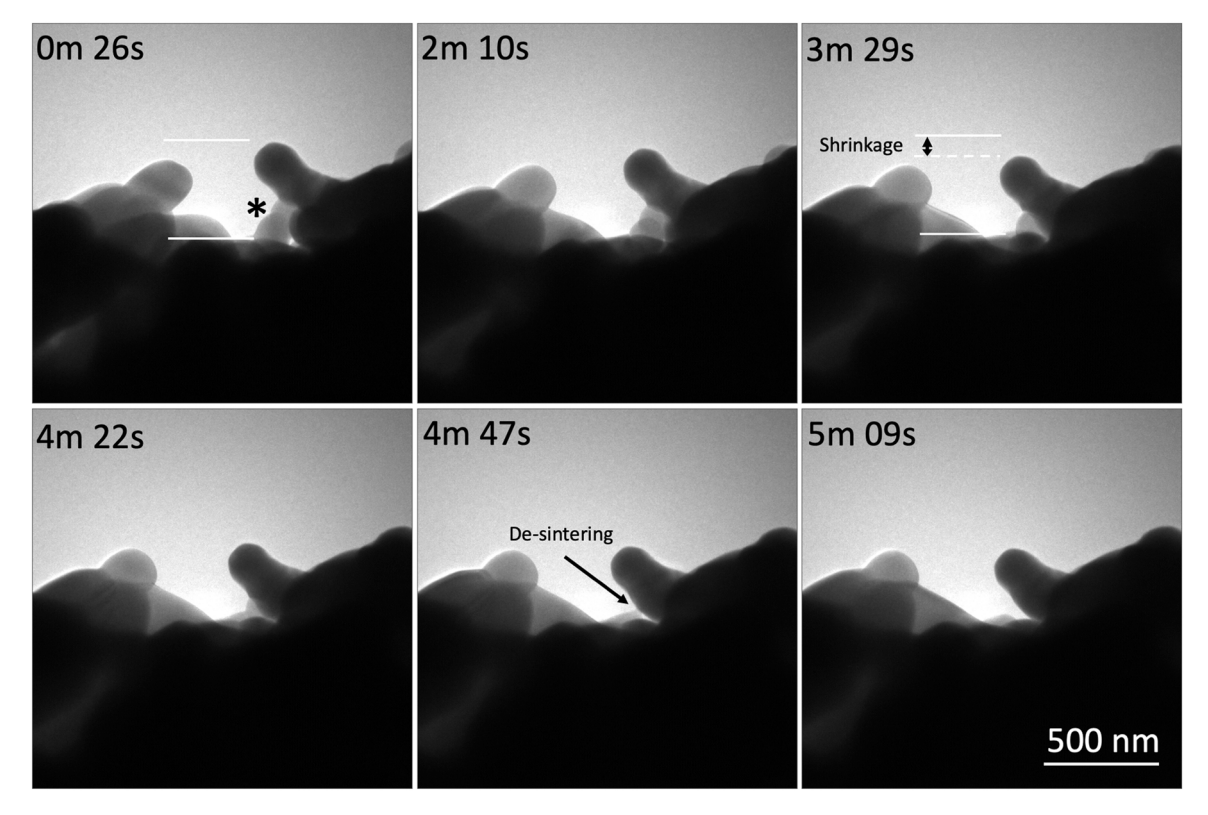


Fig. 2. Timelapse image sequence of Al_2O_3 -SmAlO₃ sintering in situ at ≈ 1440 °C. As the particles denoted by the * shrink, they induce strain between the particles attached on either side. As the particles continue to shrink, they eventually undergo a Plateau-Rayleigh (P-R) instability leading to de-sintering.

no attempt is made to separate the contributions from the two different phases to the average sintering response. The distributions of the two phases is likely to differ between analyzed clusters, which could add some scatter to the resulting data. The two particles denoted by the * rest between regions of the cluster above and below which are both contiguous with the substrate. These particles shrink continuously, and their shrinkage induces a strain of the overall structure. Supplementary Fig. S2 shows the evolution of a similar initial structure, where the shrinkage of an Al₂O₃ particle also drives densification. In classical sintering models, such bridging grains would either rapidly approach zero sintering potential, i.e. zero sintering stress, if grain boundary diffusion were facile, or would evolve towards a curvature minimizing steady-state geometry if grain boundary diffusion were zero. The net flux of mass from the shrinking grain, however, can increase the local sintering stress in both cases, which can drive the grain boundary over a nucleation barrier. The maximum local sintering stress will be defined by the grain boundary work of separation, which could be encountered if the boundary approaches a Plateau-Rayleigh (P-R) instability [68]. During a P-R instability, the average chemical potential of the system decreases due to a decrease in interfacial energy despite local increases in chemical potential at sites where pinch off ultimately occurs.

Supplementary material related to this article can be found online at doi:10.1016/j.jeurceramsoc.2023.02.058.

At t \approx 4 m 48 s in Fig. 2, the particles undergo de-sintering, followed by further shrinkage and disappearance. De-sintering is the P-R instability occurring at grain boundaries. A similar de-sintering geometry was first discussed by Sudra and Lange [69] and was recently considered in the context of the Plateau-Rayleigh (P-R) instability [70]. The inverse problem of cylindrical pore instability has also been considered in several works [71,72]. A particle resting between two particles of fixed position and shrinking continuously will always undergo a P-R instability or de-sintering [73]. If the shrinking particle rests between unconstrained particles, then the shrinking particle will induce densification at the relevant sintering stress as it shrinks. An

intermediate amount of constraint will require the shrinking particle to do mechanical work. The maximum work that may be done is given by $dG = \gamma_S dA$ and this work can be done at any stress below the grain boundary failure stress. The local stress at the grain boundary may increase via two mechanisms. First, a reduction in the grain boundary area, i.e. the sintering potential is constant and the GB area reduces. Second, coarsening could push the particle geometry away from a low energy configuration, i.e. changes in the surface curvature and dihedral angles driven by the particles volume change. For the example in Fig. 2, the P-R instability occurs when the shrinking particle no longer possesses sufficient driving force to do work of densification at the critical sintering stress. Subsequent surface energy is dissipated purely through coarsening. The importance of surface energy dissipation in determining the prevalence of sintering versus de-sintering ties the phenomena to Eq. (3), which has an equivalent energy dissipation term.

Fig. 3 and Video S2 show the evolution of a small cluster of particles at, $\approx 1130~^\circ\text{C}$ and $\approx 1370~^\circ\text{C}$. At the $\approx 1130~^\circ\text{C}$, the particles and cluster tend to exhibit a considerable amount of interfacial sliding and large angle particle rotations. Along with this re-arrangement process some de-sintering occurs. The net effect of these processes is that some regions densify, while larger pores evolve in other regions. At $\approx 1370~^\circ\text{C}$, the same cluster appears to densify more uniformly with less macroscopically observable particle rotation and rearrangement. The results highlight the role of temperature in influencing the densification strain mechanism and the evolution of internal porosity at different temperatures.

3.2. Temperature dependent sintering of large clusters

Fig. 4 presents time lapse image sequences for sintering of larger clusters of particles at $\approx 1300\,^{\circ}\text{C}, \approx 1410\,^{\circ}\text{C},$ and $\approx 1610\,^{\circ}\text{C},$ and the corresponding video data is provided in Videos S3 through 5. Qualitatively, the temperature dependence observed agrees with the results in Fig. 3. At low temperatures, the particles exhibit a larger degree of

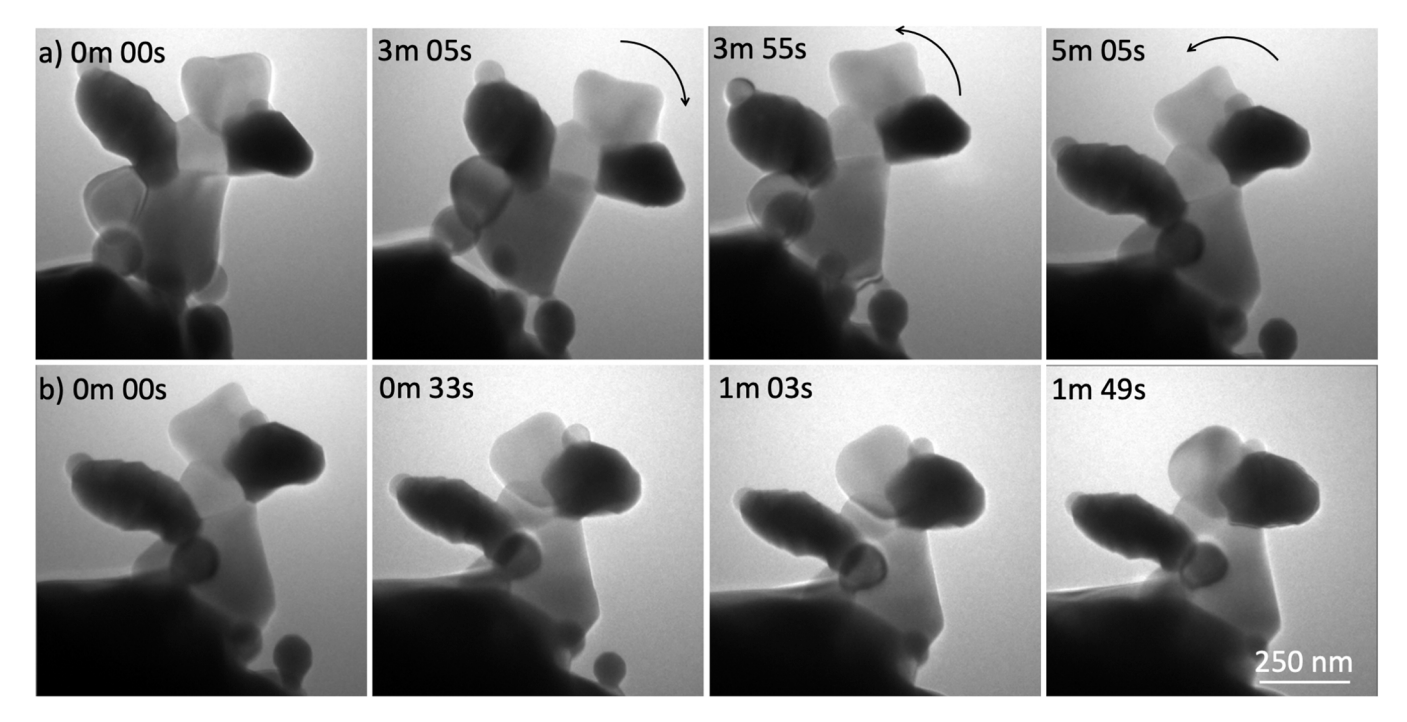


Fig. 3. Timelapse image sequences of Al_2O_3 -SmAlO $_3$ sintering in situ at (a) ≈ 1130 °C and (b) ≈ 1370 °C. The particles within this cluster undergo considerable rearrangement at the lower temperature causing observable rotation and the evolution of new larger pores, while they undergo more uniform shrinkage at the higher temperature. The dark particles are SmAlO $_3$, while the lighter particles are Al $_2O_3$.

macroscopic rotation and rearrangement, which leads to certain regions increasing in density, while other regions form larger pores. As temperature increases, this behavior is increasingly suppressed, and the particles densify more uniformly. Fig. 5(a) plots (A/V) versus ε for the data from Fig. 4. These data may be used to calculate from Eq. (3), assuming $\gamma_S \approx 1J$, $\eta \approx 0.5$, and $\zeta \approx 1$. The temperature dependence of $\sigma_{s,c}$ is plotted in Fig. 5(b), decreasing with temperature as anticipated from Eq. (2). A power law fit of $\sigma_{s,c}(T)$ is obtained for the data. The appropriate form of the equation is unclear since several parameters in Eq. (2) are unknown. In prior treatments of $\sigma_{s,c}(T)$ a linear fit was employed, primarily because the experimental scatter is large relative to an subtle variations in the data [46]. Regardless, the magnitudes of the slope, $\sigma_{s,c}(T)$ is comparable to prior measurements from low energy eutectic interfaces in Al₂O₃-GdAlO₃, and Sc₂O₃-doped ZrO₂ [37,46]. Each system produced values on the order of 106 PaK-1. Random Al₂O₃-GdAlO₃ bicrystals produce values of $\sigma_{s,c}$ comparable in magnitude to the Al₂O₃-SmAlO₃ composites tested here, [44,46] see Fig. S3. The random Al₂O₃-SmAlO₃ polycrystals tested herein, however, produce values of $\sigma_{s,c}$ lower than those measured from Al₂O₃-GdAlO₃ eutectics. The larger values of $\sigma_{s,c}$ at eutectic interfaces likely results from interfacial anisotropy associated with the lower energy eutectic interface.

Supplementary Figs. S4 and S5 present data for sets of large clusters of particles annealed for short periods of time at several, sequentially increasing temperatures. A similar qualitative trend is observed in these individual clusters; more particle rearrangement and larger rotation angles observed at lower temperatures and more uniform densification observed at higher temperatures. This indicates that the trends discussed above are not a result of differences in initial particle cluster topology but are instead related to the influence of temperature on the interfacial strain mechanisms.

The magnitude of $\sigma_{s,c}$ is quite large at lower temperatures. Thickness extinction band contours could be observed in several appropriately orientated particles. The widths of these extinction bands were found to vary in time suggesting significant time dependent variations in the elastic stress fields within the particles [74]. As shown in supplementary Fig. S6 the widths of the extinction bands were observed to oscillate

suggesting an oscillation in the stress state of the particle. This is qualitatively consistent with our expectation that the local sintering stress should increase prior to any densification or interfacial plasticity. In a few cases, the temperature of the sample was increased *in situ* and the widths of the thickness extinction bands increased consistent with a stress relaxation. This is qualitatively consistent with $\sigma_{s,c}$ decreasing with increasing temperature. In this physical picture, the interface can stabilize interfacial stresses up to $\approx \sigma_{s,c}$ and the elastic stress fields within the particle are sensitive to this interfacial stress. It is not possible, however, to disregard the possibility that the disappearance of the bands correlates with rotation of the particle.

3.3. Electron diffraction characterization of particle rotation

Electron diffraction data was obtained during in situ sintering of an individual cluster of particles at ≈ 1360 °C, ≈ 1480 °C, and ≈ 1550 °C. Fig. 6 presents images of the sample after in situ diffraction at each temperature along with a series of diffraction patterns. Associated video data are presented in Videos S6 through S8. The particle rotation rate per unit time clearly increases with increasing temperature, as the overall strain rate increases. Strain and rotation must occur cooperatively as determined by the direction of the Burger's vector relative to the grain boundary plane. Imaging indicates that the particle rotation rate per unit strain is higher at lower temperatures. The sluggish overall rate of densification at low temperatures, made it difficult to quantify this effect. The more uniform densification observed at higher temperatures, suggests that grain boundary dislocations nucleated at higher temperatures likely exhibit more climb component. The larger rotation angles at lower temperatures suggest GB dislocations in this regime exhibit more glide component.

Supplementary material related to this article can be found online at doi:10.1016/j.jeurceramsoc.2023.02.058.

4. Discussion

The sintering kinetics in Al₂O₃-SmAlO₃ generally follow the forms

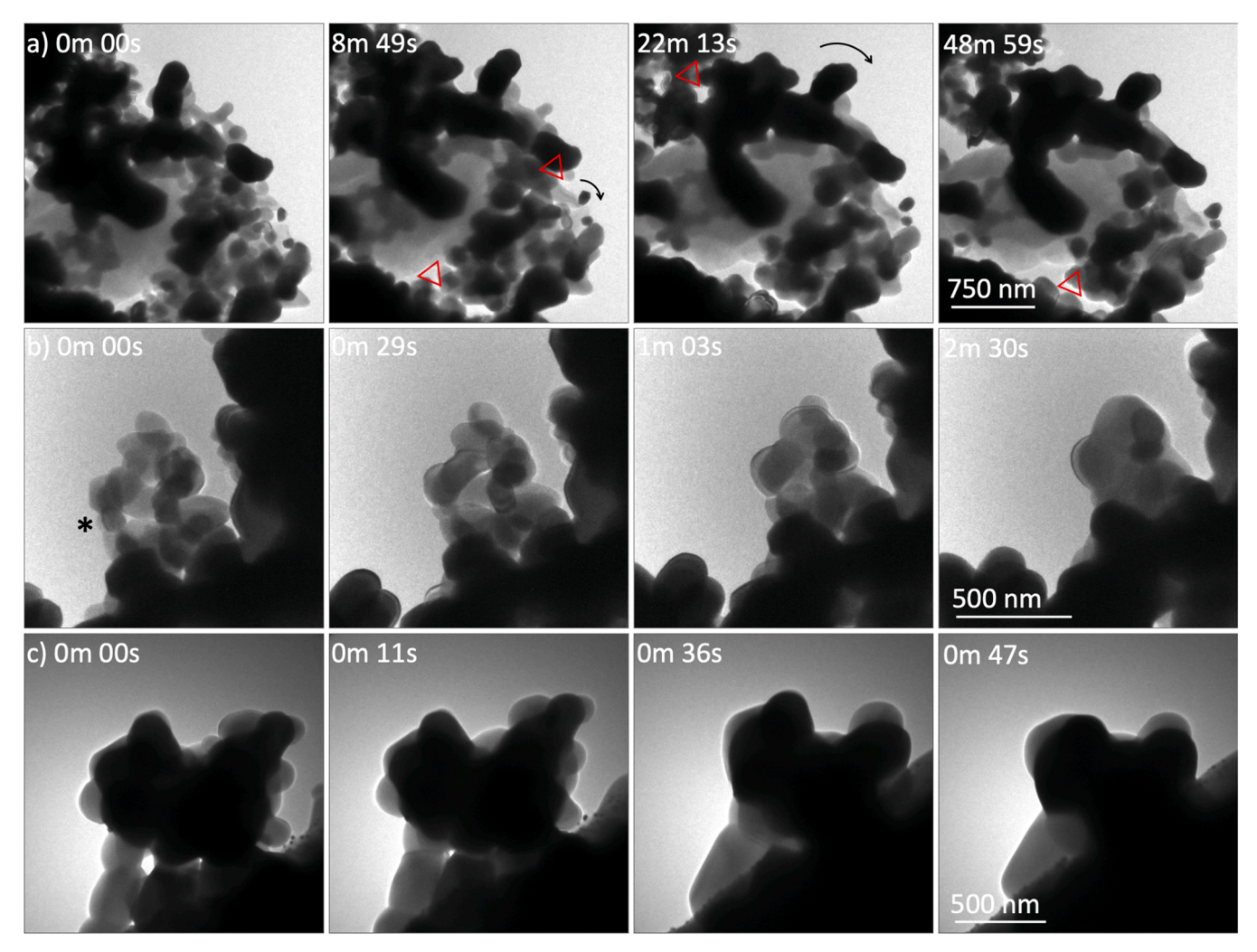


Fig. 4. Timelapse image sequences of Al_2O_3 -SmAlO $_3$ sintering in situ at (a) $\approx 1300\,^{\circ}$ C, (b) $\approx 1410\,^{\circ}$ C, and (c) $\approx 1610\,^{\circ}$ C. The triangles in (a) denote the formation of new pores because of the rearrangement process whose associated rotation is highlighted by several arrows. The structures in (b) and (c) densify more uniformly without significant macroscopic rotation. The particles denoted by the * in (b) appear to drive densification along with their shrinkages like the examples in Fig. 2 and Fig. S2. The dark particles are SmAlO $_3$, while the lighter particles are Al_2O_3 .

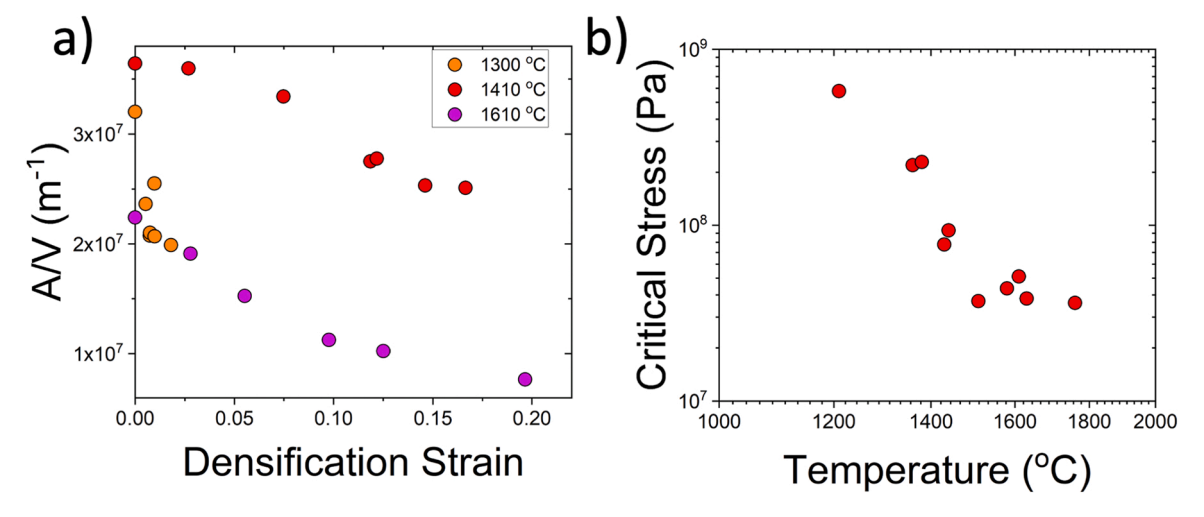


Fig. 5. (a) Plots of sintering strain versus the average ratio of particle perimeter to area, representing A/V, for the same data. (b) plot of log $\sigma_{s,c}$ versus log temperature calculated based on Eq. (3).

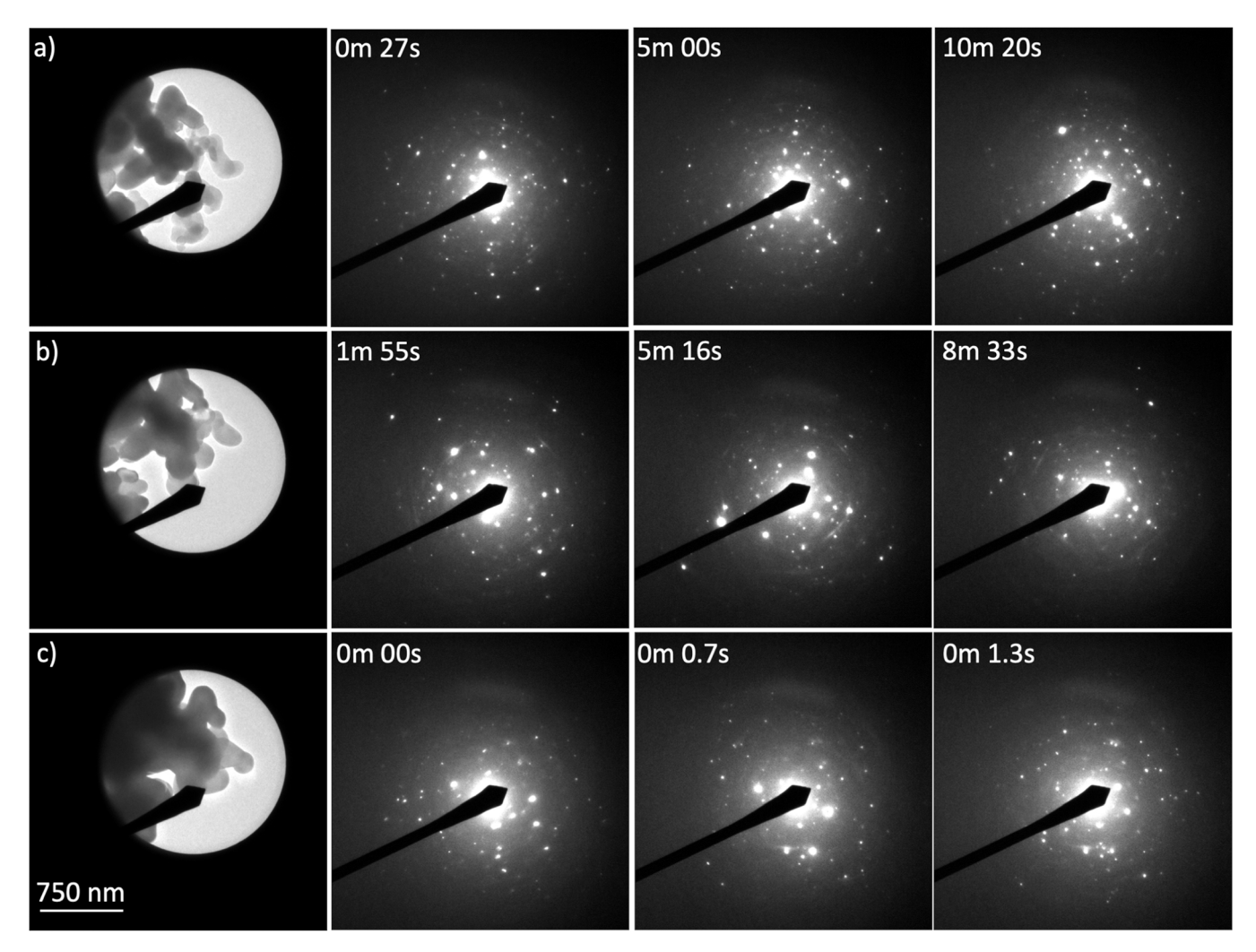


Fig. 6. Timelapse in situ electron diffraction obtained during sintering of Al_2O_3 -SmAlO $_3$ sintering at (a) ≈ 1360 °C, (b) ≈ 1480 °C, and (c) ≈ 1550 °C.

outlined in Eq. (3). $\sigma_{s,c}$ decreases with temperature as predicted by Eqs. (2) and (3). This temperature dependence is distinct from alternative models. Purely diffusive models will predict a temperature dependence of $\frac{d\varepsilon}{d(A/V)}$ if the activation energies for surface and grain boundary diffusion are sufficiently different [10,75]. In the Al₂O₃-GdAlO₃ system, which might be expected to be like Al₂O₃-SmAlO₃, these activation energies were found to be similar [45]. The temperature dependence of $\frac{d\varepsilon}{d(A/V)}$ in a diffusive model, furthermore, should not necessarily be of a particular sign, should not be of similar magnitude in different systems, and would have little physical interpretation. This and prior work [37, 38,44–46] have found, however, that $\frac{d\varepsilon}{d(A/V)}$ provides a measure of $\sigma_{s,c}$ from bicrystals and polycrystals consistent with bicrystal creep measurements of $\sigma_{s,c}$. Prior work supported the notion that the model works well at the bicrystal level, and the present results indicate that it also works well at the polycrystalline level. Nucleation rate limited densification kinetics have not been considered within the literature, thus, the implications of such a mechanism on sintering has not been sufficiently discussed. The text below focuses on considering the implications of a nucleation rate limited densification mechanisms has in interpreting commonly observed sintering phenomena.

Sintering induced particle rotation is observed here in relatively small low density clusters. Large angle particle rotation, 10–20°, has also been reported from relatively dense, 65–80%, compacts observed using *in situ* computed tomography [76]. Others have also observed particle rotations in model bicrystal experiments [77,78]. In our prior work, a

series of eutectic bicrystal boundaries of the same crystallographic character were observed as a function of temperature [46]. Like the current work, it was observed that interfacial strain occurred with larger rotation angles at lower temperatures. Some particle rotation should be inherent to densification, since random grain boundaries may be unlikely to nucleate disconnections that exhibit pure edge character. Macroscopic rotation is not observed during bicrystal grain boundary creep [38], but off axis strain is observed during bicrystal phase boundary creep [45]. Since grain boundary migration can also occur via disconnection motion [79,80], the evolution during concurrent creep and grain boundary motion is more challenging to interpret. The activation volume associated with nucleating a particular disconnection mode will be a tensor that depends on the local stress state, that is sensitive to back stresses induced by neighboring grains. The role of topology in affecting grain boundary strain is an interesting question that requires more investigation.

The effects of high heating rate and high temperature sintering have been of significant interest for several decades, since employing the methods almost universally enhance densification relative to coarsening [3–10]. Two-step sintering, wherein a sample is initial heated to high temperatures during the initial stage and then subsequently sintered at lower temperatures, is particularly interesting because it highlights the importance of initial stage sintering in affecting microstructural evolution [81]. Both two-step sintering and high heating rate high temperature sintering methods have been shown to reduce the pore size distribution [82,83], which is a critical factor affecting final stage

sintering kinetics. This link between initial stage and final stage sintering is particularly important in engineering the sintering process. The schematic in supplementary Fig. S7 highlights how de-sintering during the initial stages of sintering can affect the pore size distribution in the final stages of sintering. In this work, we demonstrate two important processes most active during the initial stages of sintering that affect the pore size distribution and provide insights into their temperature dependence. As discussed below, first, so-called particle rearrangement processes driven by particle rotation can broaden the pore size distribution via rotation of particles or clusters of particles. Second, de-sintering drives coarsening of pores when small grains approach the P-R instability during shrinkage.

Absent trapped gas within pores, the driving force for pore coarsening should be small, since a vacancy flux to a GB sink site, if it exists, will be more favorable than to a neighboring pore. Instead, pores coarsen via the de-sintering and rearrangement processes. Indeed, pore coarsening is observed during heating and initial stage sintering and is followed by subsequent pore shrinkage [82,84,85]. Particle rearrangement during sintering at low temperatures has long been known and has often been associated with the onset of densification during dilatometry experiments [86]. The process is often cited as beneficial due to the increase in density. Direct observations of such rearrangement processes in this work, however, indicate that they can broaden the pore size distribution, which is unfavorable in later stages of sintering [87]. The presence of large pores in the final stages of sintering is a key limitation on achieving full density. Low temperatures favor rearrangement due to the preference for nucleating GB dislocations with larger glide component, which are hypothesized to have lower activation energies. Applied pressure could also affect the types of GB dislocations nucleated, the amount of glide versus climb, and the rotation of particles during rearrangement. A reduction of pore size at equivalent amounts of densification has been observed for systems sintered under applied pressure [88]. Although pressure effects were not studied here, it may be reasonable to expect that suppression of rearrangement during initial stage sintering could be a benefit of stress assisted sintering methods, in addition to the enhanced driving force.

Recent simulation work [70] indicates that a P-R instability, i.e. de-sintering, will always occur at infinite time in bamboo grain structure wires of fixed length if grain growth is active. This is analogous to the fact that de-sintering will occur at 2-particle contacts if the 2 grains are shrinking and the positions of their centers of mass are fixed. To avoid de-sintering the surrounding matrix must strain at a rate faster than some critical rate below which the particle would encounter the P-R instability criterion. Since the phenomenon is sensitive to the local geometry defining a quantitative model as a function of average sample density is outside of the scope of this work. Nevertheless, it should be noted that de-sintering should become less likely when grains are coordinated by other grains, versus pores, so the process should dominate primarily during the initial stages of sintering. The ratio of the average sintering rate to the average coarsening rate, therefore, provides a metric for predicting the relative amounts of de-sintering to expect. Since $\sigma_{s,c}$ decreases with increasing temperature, as predicted from Eq. (2) and shown experimentally in Fig. 5(b), the ratio of the densification rate to coarsening rate will always be higher at higher temperatures. De-sintering will, therefore, be less favorable at higher temperatures than lower temperatures.

The unfavorable effects of de-sintering and rearrangement and their dependence on density might also play a secondary role in the well-known influence of initial density on late-stage sintering trajectory. Within the context of our model, the primary effect should come from the total strain necessary when integrating over $\frac{de}{d(A/V)}$ in Eq. (3). Desintering will be more active at lower densities since it is most likely to occur when a boundary is completely coordinated by pores. Particle rearrangement will be more favorable at lower densities due to the large free volume in the system. Eq. (3) includes a term ζ that describes the

efficiency of converting interfacial energy dissipation during coarsening into work on densification. De-sintering will reduce the magnitude of ζ , but this is anticipated to be a secondary effect in the initial stages where the amount of de-sintering is small relative to the amount of sintering.

 ζ in Eq. (3) will also affect the final stages of sintering. As the relative density of the sample goes to 1, ζ must go to zero. Interfacial energy dissipation at grains not coordinated by pores, clearly, will not affect densification. To predictively apply Eq. (3) to the final stages of sintering, an improved mechanistic understanding of the co-evolution of pore size and grain size distribution must be developed. The current work represents an initial assessment of the processes active in driving pore coarsening during the initial stages of sintering. Theoretical models describing both the distributions of GB dislocation nucleation activation energies and activation volumes, as well as the P-R instability in complex geometries will need to be developed to predict how sintering process variables affect microstructural evolution.

Classical treatments of sintering assume that densification and coarsening occur independently and compete to dissipate interfacial energy. The model outlined herein implies that densification depends directly on coarsening to overcome nucleation barriers. The relationship between the processes induces broad trends observed within the sintering literature, such as the beneficial effects of high heating rates, high temperature annealing during the initial stage of sintering, a temperature dependence to residual stress evolution, and sintering strain rates that exceed creep strain rates at equivalent average driving forces. From this point, an improved understanding of sintering phenomena may be obtained by better understanding the relationship between local microstructure and our model.

5. Conclusions

In situ sintering of particle clusters indicates that $\frac{de}{d(A/V)} = -\frac{r_S \xi}{\sigma_{s,c}\eta}$ fits polycrystalline data well. The magnitude of $\sigma_{s,c}$, calculated by fitting the model to the experiments, decreases with temperature. This is consistent with observations of thickness extinction band contours that suggest the particles are under higher stresses at lower temperatures. The temperature dependence of $\sigma_{s,c}$ influences the propensity for particle rotation, associate particle rearrangement, and de-sintering at different temperatures. In contrast to classical theory, this study suggests that densification depends directly on coarsening to overcome nucleation barriers during sintering. These coupled effects could account for the efficacy of employing high heating rates and high temperature annealing during the initial stages of sintering.

Declaration of Competing Interest

The authors declare that they have no known competing financial interests or personal relationships that could have appeared to influence the work reported in this paper.

Acknowledgments

Support from National Science Foundation under Grant DMR 1922867 is acknowledged by K.C and S.J.D. E.L. and K.H. were supported by the DOE-BES Materials Science and Engineering Division under FWP 15013170. This work was performed, in part, at the Center for Integrated Nanotechnologies, an Office of Science User Facility operated for the U.S. Department of Energy (DOE) Office of Science. Sandia National Laboratories is a multimission laboratory managed and operated by National Technology and Engineering Solutions of Sandia, LLC, a wholly owned subsidiary of Honeywell International, Inc., for the U.S. DOE's National Nuclear Security Administration under contract DE-NA-0003525. The views expressed in the article do not necessarily represent the views of the U.S. DOE or the United States Government. Y. H.M acknowledges support from the Fundamental Research Funds for

the Central Universities under No. 3072022TS2702 and J.h.O. acknowledge Natural Science Foundation of China for the supports in this work under Grant Nos. 51972085, 51572061 and 51621091.

Appendix A. Supporting information

Supplementary data associated with this article can be found in the online version at doi:10.1016/j.jeurceramsoc.2023.02.058.

References

- J. Lewis, S. Dillon, K. Sun, B.Y. Ahn, T.-S. Wei, Three-Dimensional (3d) Electrode Architecture for A Microbattery, University of Illinois,, USA, 2014, p. 37.
- [2] J.A. Lewis, Direct ink writing of 3D functional materials, Adv. Funct. Mater. 16 (2006) 2193–2204.
- [3] C. Wang, W. Ping, Q. Bai, H. Cui, R. Hensleigh, R. Wang, A.H. Brozena, Z. Xu, J. Dai, Y. Pei, C. Zheng, G. Pastel, J. Gao, X. Wang, H. Wang, J.-C. Zhao, B. Yang, X. Zheng, J. Luo, Y. Mo, B. Dunn, L. Hu, A general method to synthesize and sinter bulk ceramics in seconds, Science 368 (6490) (2020) 521–526, https://doi.org/10.1126/science.aaz7681
- [4] M. Cologna, B. Rashkova, R. Raj, Flash sintering of nanograin zirconia in <5 s at 850°C, J. Am. Ceram. Soc. 93 (11) (2010) 3556–3559, https://doi.org/10.1111/ i.1551-2916.2010.04089.x.
- [5] S.K. Jha, R. Raj, Electric fields obviate constrained sintering, J. Am. Ceram. Soc. 97 (10) (2014) 3103–3109, https://doi.org/10.1111/jace.13136.
- [6] S.J. Penn, N.M. Alford, A. Templeton, X. Wang, M. Xu, M. Reece, K. Schrapel, Effect of porosity and grain size on the microwave dielectric properties of sintered alumina, J. Am. Ceram. Soc. 80 (7) (1997) 1885–1888.
- [7] W. Li, L. Gao, Rapid sintering of nanocrystalline ZrO₂(3Y) by spark plasma sintering, J. Eur. Ceram. Soc. 20 (14–15) (2000) 2441–2445, https://doi.org/ 10.1016/S0955-2219(00)00152-7.
- [8] W. Ji, B. Parker, S. Falco, J.Y. Zhang, Z.Y. Fu, R.I. Todd, Ultra-fast firing: effect of heating rate on sintering of SYSZ, with and without an electric field, J. Eur. Ceram. Soc. 37 (6) (2017) 2547–2551, https://doi.org/10.1016/j. jeurceramsoc.2017.01.033.
- [9] L. Porz, M. Scherer, D. Huhn, L.-M. Heine, S. Britten, L. Rebohle, M. Neubert, M. Brown, P. Lascelles, R. Kitson, D. Rettenwander, L. Fulanovic, E. Bruder, P. Breckner, D. Isaia, T. Frömling, J. Rödel, W. Rheinheimer, Blacklight sintering of ceramics, Mater. Horiz. 9 (6) (2022) 1717–1726, https://doi.org/10.1039/ D2MH00177B.
- [10] M. Harmer, E.W. Roberts, R.J. Brook, Rapid sintering of pure and doped α -alumina, Trans. J. Br. Ceram. Soc. 78 (1) (1979) 22–25.
- [11] R.L. Coble, Initial sintering of alumina and hematite, J. Am. Ceram. Soc. 41 (1958) 55–62, https://doi.org/10.1111/j.1151-2916.1958.tb13519.x.
- [12] R.L. Coble, Sintering crystalline solids. II. Experimental test of diffusion models in powder compacts, J. Appl. Phys. 32 (1961) 793–799, https://doi.org/10.1063/ 1.1736108.
- [13] R.L. Coble, Sintering crystalline solids. I. Intermediate- and final-state diffusion models, J. Appl. Phys. 32 (1961) 787–792, https://doi.org/10.1063/1.1736107.
- [14] D.L. Johnson, I.B. Cutler, Diffusion sintering. I. Initial stage sintering models and their application to shrinkage of powder compacts, J. Am. Ceram. Soc. 46 (11) (1963) 541–545, https://doi.org/10.1111/j.1151-2916.1963.tb14606.x.
- [15] D.L. Johnson, New method of obtaining volume, grain-boundary, and surface diffusion coefficients from sintering data, J. Appl. Phys. 40 (1) (1969) 192–200, https://doi.org/10.1063/1.1657030.
- [16] G.C. Kuczynski, Self-diffusion in sintering of metallic particles, Trans. Am. Inst. Min. Metall. Pet. Eng. 1 (No. 2, Trans.) (1949) 169–178.
- [17] Z. He, J. Ma, Constitutive modelling of the densification of micron-grain-sized alumina ceramics, Philos. Mag. 83 (16) (2003) 1889–1916, https://doi.org/ 10.1080/1478643031000107267.
- [18] Z.Z. Du, A.C.F. Cocks, Constitutive models for the sintering of ceramic components—I. Material models, Acta Metall. Et. Mater. 40 (8) (1992) 1969–1979, https://doi.org/10.1016/0956-7151(92)90183-F.
- [19] S. Mao, S. Shu, J. Zhou, R.S. Averback, S.J. Dillon, Quantitative comparison of sink efficiency of Cu-Nb, Cu-V and Cu-Ni interfaces for point defects, Acta Mater. 82 (2015) 328–335, https://doi.org/10.1016/j.actamat.2014.09.011.
- [20] R.W. Siegel, S.M. Chang, R.W. Balluffi, Vacancy loss at grain boundaries in quenched polycrystalline gold, Acta Metall. 28 (3) (1980) 249–257, https://doi. org/10.1016/0001-6160(80)90159-5.
- [21] P.B. Hirsch, J. Silcox, R.E. Smallman, K.H. Westmacott, Dislocation loops in quenched aluminium, Philos. Mag. A J. Theor. Exp. Appl. Phys. 3 (32) (1958) 897–908, https://doi.org/10.1080/14786435808237028.
- [22] M.F. Ashby, Interface-reaction control of Nabarro-Herring creep and sintering, Scr. Met. 3 (11) (1969) 837–842, https://doi.org/10.1016/0036-9748(69)90191-4.
- [23] R.L. Coble, A model for boundary diffusion controlled creep in polycrystalline materials, J. Appl. Phys. 34 (6) (1963) 1679–1682, https://doi.org/10.1063/ 1.1702656
- [24] E. Arzt, M.F. Ashby, R.A. Verrall, Interface controlled diffusional creep, Acta Metall. 31 (12) (1983) 1977–1989, https://doi.org/10.1016/0001-6160(83) 90015-9.
- [25] B. Burton, Interface reaction controlled diffusional creep: a consideration of grain boundary dislocation climb sources, Mater. Sci. Eng. 10 (1972) 9–14, https://doi. org/10.1016/0025-5416(72)90060-2.

- [26] R.M. Cannon, W.H. Rhodes, A.H. Heuer, Plastic deformation of fine-grained alumina (Al2O3): I, interface-controlled diffusional creep, J. Am. Ceram. Soc. 63 (1–2) (1980) 46–53, https://doi.org/10.1111/j.1151-2916.1980.tb10648.x.
- [27] B. Burton, G.L. Reynolds, The diffusional creep of uranium dioxide: its limitation by interfacial processes, Acta Metall. 21 (8) (1973) 1073–1078, https://doi.org/ 10.1016/0001-6160(73)90023-0.
- [28] D. Lahiri, S.V.R. Rao, G.V.S.H. Rao, R.K. Srivastava, Study on sintering kinetics and activation energy of UO₂ pellets using three different methods, J. Nucl. Mater. 357 (1) (2006) 88–96, https://doi.org/10.1016/j.jnucmat.2006.05.046.
- [29] J.L. Woolfrey, Effect of green density on the initial-stage sintering kinetics of UO2s, J. Am. Ceram. Soc. 55 (8) (1972) 383–389, https://doi.org/10.1111/j.1151-2916.1972.tb11318.x.
- [30] M. Boniecki, Z. Librant, A. Wajler, W. Wesołowski, H. Węglarz, Fracture toughness, strength and creep of transparent ceramics at high temperature, Ceram. Int. 38 (6) (2012) 4517–4524, https://doi.org/10.1016/j.ceramint.2012.02.028.
- [31] T.A. Parthasarathy, T.-I. Mah, K. Keller, Creep mechanism of polycrystalline yttrium aluminum garnet, J. Am. Ceram. Soc. 75 (7) (1992) 1756–1759, https://doi.org/10.1111/j.1151-2916.1992.tb07193.x.
- [32] A. Talimian, H.F. El-Maghraby, M. Michálková, D. Galusek, Sintering and grain growth behaviour of magnesium aluminate spinel: effect of lithium hydroxide addition, J. Eur. Ceram. Soc. 41 (11) (2021) 5634–5643, https://doi.org/10.1016/ i.jeurceramsoc.2021.05.003.
- [33] C.-J. Ting, H.-Y. Lu, Defect reactions and the controlling mechanism in the sintering of magnesium aluminate spinel, J. Am. Ceram. Soc. 82 (4) (1999) 841–848, https://doi.org/10.1111/j.1151-2916.1999.tb01844.x.
- [34] B. Burton, G.W. Greenwood, The contribution of grain-boundary diffusion to creep at low stresses, Met. Sci. J. 4 (1) (1970) 215–218, https://doi.org/10.1179/ msc.1970.4.1.215.
- [35] D. Demirskyi, D. Agrawal, A. Ragulya, Densification kinetics of powdered copper under single-mode and multimode microwave sintering, Mater. Lett. 64 (13) (2010) 1433–1436, https://doi.org/10.1016/j.matlet.2010.03.047.
- [36] C.-J. Ting, H.-Y. Lu, Hot-pressing of magnesium aluminate spinel—I. Kinetics and densification mechanism1This paper is based in part on the thesis submitted by C.-J. Ting in 1997 to National Sun Yat-Sen University in partial fulfilment of the requirements for Ph.D.1, Acta Mater. 47 (3) (1999) 817–830, https://doi.org/ 10.1016/S1359-6454(98)00400-5.
- [37] R.L. Grosso, K.S.N. Vikrant, L. Feng, E.N.S. Muccillo, D.N.F. Muche, G. S. Jawaharram, C.M. Barr, A.M. Monterrosa, R.H.R. Castro, R.E. Garcia, K. Hattar, S.J. Dillon, Ultrahigh temperature in situ transmission electron microscopy based bicrystal coble creep in Zirconia II: Interfacial thermodynamics and transport mechanisms, Acta Mater. 200 (2020) 1008–1021, https://doi.org/10.1016/j.actamat.2020.08.070.
- [38] K.S.N. Vikrant, R.L. Grosso, L. Feng, E.N.S. Muccillo, D.N.F. Muche, G. S. Jawaharram, C.M. Barr, A.M. Monterrosa, R.H.R. Castro, R.E. Garcia, K. Hattar, S.J. Dillon, Ultrahigh temperature in situ transmission electron microscopy based bicrystal coble creep in zirconia I: Nanowire growth and interfacial diffusivity, Acta Mater. 199 (2020) 530–541, https://doi.org/10.1016/j.actamat.2020.08.069.
- [39] B. Sudhir, A.H. Chokshi, Compression creep characteristics of 8-mol%-Yttriastabilized cubic-zirconia, J. Am. Ceram. Soc. 84 (11) (2001) 2625–2632, https:// doi.org/10.1111/j.1151-2916.2001.tb01063.x.
- [40] A.S. Argon, Intergranular cavitation in creeping alloys, Scr. Metall. 17 (1) (1983) 5–12, https://doi.org/10.1016/0036-9748(83)90061-3.
- [41] R. Raj, M.F. Ashby, Intergranular fracture at elevated temperature, Acta Metall. 23 (6) (1975) 653–666, https://doi.org/10.1016/0001-6160(75)90047-4.
- [42] H. Trinkaus, M.H. Yoo, Cavity nucleation under time-dependent stress concentrations, Philos. Mag. A 57 (4) (1988) 543–564, https://doi.org/10.1080/ 01418618808214406.
- [43] S.J. Dillon, E. Lang, S.C. Finkeldei, J.-H Ouyang, K. Hattar, A nucleation rate limited model for grain boundary creep, Acta Mater. (2023), 118718, https://doi. org/10.1016/j.actamat.2023.118718.
- [44] D.K. Coffman, Y. Ma, C. Barr, J.-H. Ouyang, K. Hattar, S.J. Dillon, Evidence for interface-rate limited densification kinetics at Al₂O₃-GdAlO₃ interfaces characterized by in situ ultrahigh temperature transmission electron microscopy, J. Eur. Ceram. Soc. (2022), https://doi.org/10.1016/j.jeurceramsoc.2022.06.001.
- [45] D.K. Coffman, Y. Ma, C.M. Barr, J.-h Ouyang, K. Hattar, S.J. Dillon, Interphase boundary, grain boundary, and surface diffusion in Al₂O₃/GdAlO₃ composites determined from bicrystal coble creep experiments, J. Eur. Ceram. Soc. 42 (9) (2022) 3976–3985, https://doi.org/10.1016/j.jeurceramsoc.2022.02.052.
- [46] S.J. Dillon, Y. Ma, J.-h Oyang, O. Husseind, K. Hattar, F. Abdeljawadd, Interface nucleation rate limited densification during sintering. Acta Mater. (2022) https:// doi.org/10.1016/j.actamat.2022.118448.
- [47] O. Hussein, M. Alghalayini, S.J. Dillon, F. Abdeljawad, Unraveling the role of grain boundary anisotropy in sintering: implications for nanoscale manufacturing, ACS Appl. Nano Mater. 4 (8) (2021) 8039–8049, https://doi.org/10.1021/ acsanm.1c01322.
- [48] G. Taylor, Thermally-activated deformation of BCC metals and alloys, Prog. Mater. Sci. 36 (1992) 29–61, https://doi.org/10.1016/0079-6425(92)90004-Q.
- [49] F.A. Nichols, W.W. Mullins, Morphological changes of a surface of revolution due to capillarity-induced surface diffusion, J. Appl. Phys. 36 (6) (1965) 1826–1835, https://doi.org/10.1063/1.1714360.
- [50] W.K. Burton, N. Cabrera, F.C. Frank, N.F. Mott, The growth of crystals and the equilibrium structure of their surfaces, Philos. Trans. R. Soc. Lond. Ser. A, Math. Phys. Sci. 243 (866) (1951) 299–358, https://doi.org/10.1098/rsta.1951.0006.
- [51] T. Schober, R.W. Balluffi, Grain boundary dislocation spirals in high-angle (001) twist boundaries in gold, Philos. Mag. A J. Theor. Exp. Appl. Phys. 24 (188) (1971) 469–474, https://doi.org/10.1080/14786437108227401.

- [52] T. Schober, R.W. Balluffi, Extraneous grain boundary dislocations in low and high angle (001) twist boundaries in gold, Philos. Mag.: A J. Theor. Exp. Appl. Phys. 24 (187) (1971) 165–180, https://doi.org/10.1080/14786437108216431.
- [53] H. Gleiter, The mechanism of grain boundary migration, Acta Metall. 17 (5) (1969) 565–573, https://doi.org/10.1016/0001-6160(69)90115-1.
- [54] R.M. Cannon, W.C. Carter, Interplay of sintering microstructures, driving forces, and mass transport mechanisms, J. Am. Ceram. Soc. 72 (8) (1989) 1550–1555, https://doi.org/10.1111/j.1151-2916.1989.tb07705.x.
- [55] J. Han, S.L. Thomas, D.J. Srolovitz, Grain-boundary kinetics: a unified approach, Prog. Mater. Sci. 98 (2018) 386–476, https://doi.org/10.1016/j. pmatsci.2018.05.004.
- [56] S.E. Babcock, R.W. Balluffi, Grain boundary kinetics—I. In situ observations of coupled grain boundary dislocation motion, crystal translation and boundary displacement, Acta Metall. 37 (9) (1989) 2357–2365, https://doi.org/10.1016/ 0001-6160(89)90033-3.
- [57] Y.-H. Ma, Z.-G. Wang, J.-H. Ouyang, S.J. Dillon, A. Henniche, Y.-H. Wang, Y.-J. Wang, Microstructural toughening mechanisms in nanostructured Al₂O₃/GdAlO₃ eutectic composite studied using in situ microscale fracture experiments, J. Eur. Ceram. Soc. 40 (8) (2020) 3148–3157, https://doi.org/10.1016/j.jeurceramsoc.2020.02.042.
- [58] Y. Waku, N. Nakagawa, T. Wakamoto, H. Ohtsubo, K. Shimizu, Y. Kohtoku, A ductile ceramic eutectic composite with high strength at 1,873 K, Nature 389 (6646) (1997) 49–52, https://doi.org/10.1038/37937.
- [59] A. Sayir, S.C. Farmer, The effect of the microstructure on mechanical properties of directionally solidified Al₂O₃/ZrO₂(Y₂O₃) eutectic, Acta Mater. 48 (18/19) (2000) 4691–4697, https://doi.org/10.1016/S1359-6454(00)00259-7.
- [60] P.B. Oliete, J.I. Pena, A. Larrea, V.M. Orera, J.L. Lorca, J.Y. Pastor, A. Martin, J. Segurado, Ultra-high-strength nanofibrillar Al₂O₃-YAG-YSZ eutectics, Adv. Mater. 19 (17) (2007) 2313–2318, https://doi.org/10.1002/adma.200602379.
- [61] T. Mah, T.A. Parthasarathy, and L.E. Matson, Processing and Mechanical Properties of Al2O3/Y3Al5O12 (YAG) Eutectic Composite, in 14th Annual Conference on Composites and Advanced Ceramic Materials: Ceramic Engineering and Science Proceedings. 1990. p. 1617–1627. https://doi.org/10.1002/9780470313053. ch36.
- [62] J. Ouyang, Y. Ma, A. Henniche, B. Wang, Z. Wang, Y. Wang, Synthesis, densification and characterization of nanosized oxide ceramic powders with eutectic compositions by heating of alcohol–aqueous salt solutions, J. Ceram. Sci. Technol. 8 (2017) 81–90.
- [63] S.J. Dillon, M. Tang, W.C. Carter, M.P. Harmer, Complexion: a new concept for kinetic engineering in materials science, Acta Mater. 55 (18) (2007) 6208–6218, https://doi.org/10.1016/j.actamat.2007.07.029.
- [64] G.S. Jawaharram, P.M. Price, C.M. Barr, K. Hattar, R.S. Averback, S.J. Dillon, High temperature irradiation induced creep in Ag nanopillars measured via in situ transmission electron microscopy, Scr. Mater. 148 (2018) 1–4, https://doi.org/ 10.1016/j.scriptamat.2018.01.007.
- [65] G.S. Jawaharram, C.M. Barr, A.M. Monterrosa, K. Hattar, R.S. Averback, S. J. Dillon, Irradiation induced creep in nanocrystalline high entropy alloys, Acta Mater. 182 (2020) 68–76, https://doi.org/10.1016/j.actamat.2019.10.022.
- [66] G.P. Pells, Radiation damage effects in alumina, J. Am. Ceram. Soc. 77 (2) (1994) 368–377, https://doi.org/10.1111/j.1151-2916.1994.tb07004.x.
- [67] K.W. Noh, Y. Liu, L. Sun, S.J. Dillon, Challenges associated with in-situ TEM in environmental systems: The case of silver in aqueous solutions, Ultramicroscopy 116 (2012) 34–38, https://doi.org/10.1016/j.ultramic.2012.03.012.
- [68] L. Rayleigh, On the instability of jets, Proc. Lond. Math. Soc. s1–10 (1) (1878) 4–13, https://doi.org/10.1112/plms/s1-10.1.4.
- [69] O. Sudre, F.F. Lange, The effect of inclusions on densification: III, the desintering phenomenon, J. Am. Ceram. Soc. 75 (12) (1992) 3241–3251, https://doi.org/ 10.1111/j.1151-2916.1992.tb04417.x
- [70] O. Hussein, D.K. Coffman, K. Hattar, E. Lang, S.J. Dillon, F. Abdeljawad, Plateau–Rayleigh instability with a grain boundary twist. submitted.

- [71] T. Spusta, J. Svoboda, K. Maca, Study of pore closure during pressure-less sintering of advanced oxide ceramics, Acta Mater. 115 (2016) 347–353, https://doi.org/ 10.1016/j.actamat.2016.05.049.
- [72] W.C. Carter, A.M. Glaeser, The morphological stability of continuous intergranular phases: Thermodynamic considerations, Acta Metall. 35 (1) (1987) 237–245, https://doi.org/10.1016/0001-6160(87)90231-8.
- [73] F.F. Lange, De-sintering, a phenonmena concurrent with densifictation within powder compacts: a review, in: R.M. German, G.L. Messing, R.G. Cornwall (Eds.), Sintering Technology, Marcel Dekker, New York, 1996.
- [74] R.Z. Valiev, R.K. Islamgaliev, I.V. Alexandrov, Bulk nanostructured materials from severe plastic deformation, Prog. Mater. Sci. 45 (2) (2000) 103–189, https://doi. org/10.1016/S0079-6425(99)00007-9.
- [75] M.P. Harmer, R.J. Brook, The effect of magnesia additions on the kinetics of hot pressing in alumina, J. Mater. Sci. 15 (12) (1980) 3017–3024, https://doi.org/ 10.1007/BF00550370
- [76] S.A. McDonald, C. Holzner, E.M. Lauridsen, P. Reischig, A.P. Merkle, P.J. Withers, Microstructural evolution during sintering of copper particles studied by laboratory diffraction contrast tomography (LabDCT), Sci. Rep. 7 (1) (2017) 5251, https://doi.org/10.1038/s41598-017-04742-1.
- [77] F. Wakai, H. Fukutome, N. Kobayashi, T. Misaki, Y. Shinoda, T. Akatsu, M. Sone, Y. Higo, Direct observation of sintering mechanics of a single grain boundary, Acta Mater. 60 (2) (2012) 507–516, https://doi.org/10.1016/j.actamat.2011.10.003.
- [78] B. Kieback, M. Noethe, R. Grupp, J. Banhart, T. Rasp, T. Kraft, Analysis of particle rolling and intrinsic rotations in copper powder during sintering, J. Mater. Sci. 47 (20) (2012) 7047–7055, https://doi.org/10.1007/s10853-012-6558-0.
- [79] M. Salvalaglio, D.J. Srolovitz, J. Han, Disconnection-Mediated migration of interfaces in microstructures: II. diffuse interface simulations, Acta Mater. 227 (2022), 117463, https://doi.org/10.1016/j.actamat.2021.117463.
- [80] J. Han, D.J. Srolovitz, M. Salvalaglio, Disconnection-mediated migration of interfaces in microstructures: I. continuum model, Acta Mater. 227 (2022), 117178, https://doi.org/10.1016/j.actamat.2021.117178.
- [81] I.W. Chen, X.H. Wang, Sintering dense nanocrystalline ceramics without final-stage grain growth, Nature 404 (6774) (2000) 168–171, https://doi.org/10.1038/ 35004548
- [82] D.-H. Kim, C.H. Kim, Effect of heating rate on pore shrinkage in yttria-doped zirconia, J. Am. Ceram. Soc. 76 (7) (1993) 1877–1878, https://doi.org/10.1111/ i.1151-2916.1993.tb06665.x.
- [83] T. Isobe, A. Ooyama, M. Shimizu, A. Nakajima, Pore size control of Al₂O₃ ceramics using two-step sintering, Ceram. Int. 38 (1) (2012) 787–793, https://doi.org/ 10.1016/j.ceramint.2011.08.005.
- [84] J.A. Varela, O.J. Whittemore, E. Longo, Pore size evolution during sintering of ceramic oxides, Ceram. Int. 16 (3) (1990) 177–189, https://doi.org/10.1016/ 0272-8842(90)90053-I.
- [85] O.J. Whittemore, J.J. Sipe, Pore growth during the initial stages of sintering ceramics, Powder Technol. 9 (4) (1974) 159–164, https://doi.org/10.1016/0032-5910(74)80027-6.
- [86] P.-L. Chen, I.W. Chen, Sintering of fine oxide powders: II, sintering mechanisms, J. Am. Ceram. Soc. 80 (3) (1997) 637–645, https://doi.org/10.1111/j.1151-2916.1997.tb02879.x.
- [87] I.W. Chen, G.N. Hassold, D.J. Srolovitz, Computer simulation of final-stage sintering: II, influence of initial pore size, J. Am. Ceram. Soc. 73 (10) (1990) 2865–2872, https://doi.org/10.1111/j.1151-2916.1990.tb06687.x.
- [88] K.A. Khor, Hot isostatic pressing modifications of pore size distribution in plasma sprayed coatings, Mater. Manuf. Process. 12 (2) (1997) 291–307, https://doi.org/ 10.1080/10426919708935142.
- [89] M.S. Seltzer, P.K. Talty, High-temperature creep of Y₂O₃-stabilized ZrO₂, J. Am. Ceram. Soc. 58 (3–4) (1975) 124–130, https://doi.org/10.1111/j.1151-2016.1975 bi.1574 v
- [90] A.G. Karaulov, I.N. Rudyak, Sintering zirconia with yttrium oxide, Refractories 16 (1) (1975) 123–127, https://doi.org/10.1007/BF01287903.